High Density, Transparent, Flexible, Microelectrode Array for Multimodal Cardiac Monitoring

by Amy Fehr

B.S in Biomedical Engineering, May 2024, The George Washington University

A Thesis submitted to

The Faculty of
The School of Engineering and Applied Science
of The George Washington University
in partial fulfillment of the requirements
for the degree of Master of Science

May 18th, 2025

Thesis directed by

Luyao Lu
Associate Professor of Biomedical Engineering

© Copyright 2025 by Amy Fehr
All rights reserved

Acknowledgments

I would like to thank Dr. Lu for his patience and guidance throughout both this process and my entire research journey at GW, which has been one of the foundational experiences of my time here. I would also like to thank all the members of my examining committee, Dr. Li, Dr. Choe, and Dr. Krauthamer, for taking time out of their schedules to help me in this process. I would like to thank all the members of my lab, current and former, for all they have taught me and all the effort they have put into my training and education. In particular, I would like to thank Jimmy Chen and Nathaniel Quirion, without whom I would not be defending a master's thesis. I would like to thank Dr. Nicole Charles in the GWU Nanofabrication and Imaging Center who so tirelessly maintains the equipment that enables this work. Lastly, I would like to thank my friends and my family who have never hesitated to support and encourage me throughout this project and my time at The George Washington University.

Abstract of Thesis

High Density, Transparent, Flexible, Microelectrode Array for Multimodal Cardiac Monitoring

The use of microelectrode arrays (MEAs) has revolutionized the study, diagnosis, and treatment of cardiac disease. The observation of electrical wave propagation through heart tissue and analysis of the individual cell populations that contribute to this phenomenon requires a robust network of high-density recording electrodes. While MEAs facilitate the study of electrical wave propagation on this scale, electrical behavior alone is no longer sufficient to fully understand the complex mechanisms underlying cardiac disease. There is also a wealth of information to be gained from optical studies of the heart, including optogenetics, or traditional dye-based fluorescence studies. The acknowledgement of cardiac disease as a complex, multiparametric issue has resulted in a desire to combine the electrical recording properties of an MEA with optical studies to achieve co-localized, simultaneous optical and electrical recording. However, the opacity of flat metal electrodes traditionally used in MEA fabrication proves to be a significant challenge in this effort. Opaque metal electrodes obscure the tissue beneath the electrode measurement site and create optical interference artifacts which result in skewed, incomplete optical data sets. The solution to this problem has been found in the form of transparent conductive materials, such as indium tin oxide and graphene. While still conductive, these materials are highly transparent, allowing electrical measurements to be made at the same time as optical measurements, with little fear of obstruction. However, these materials suffer from poor mechanical performance, leading to defects and damage

when attached to the constantly mobile tissue of the heart, and are often too expensive to be practical in many applications. This paper investigates silver nanowire as a low cost, high electrical performance, high transmittance, highly flexible alternative to other transparent conductors. We present a 64 channel silver nanowire based MEA which achieves both an impedance of 29.5 kΩ at 1 kHz and an average transmittance of 88.5%, indicating strong potential for optoelectronic applications. Moreover, the use of hyper flexible substrates to support the device allowed it to withstand 5000 bending cycles around a 5 mm radius with no significant degradation of its electrical performance, indicating its ability to withstand use on beating cardiac tissue. Gold electroplating of silver nanowire electrodes was also investigated as a way to protect tissue from the cytotoxic effects of silver and protect the electrodes themselves against oxidation without sacrificing the transmittance of the device. Electroplating silver nanowire with gold for 10 seconds was found to protect the film from oxidation, demonstrating complete gold coverage without a significant sacrifice in transmittance. This paper presents a simple, versatile approach for the fabrication of a high density, flexible, transparent microelectrode array suitable for optoelectronic integration and a broad range of cardiac applications.

Table of Contents

Acknowledgments iii

Abstract iv

Table of Contents vi

List of Figures viii

Chapter 1: Introduction 1

1.1 Cardiac Disease and the Mechanisms of Heart Function 1

1.2 Cardiac Monitoring 3

1.2.1 Electrical Cardiac Monitoring 4

1.2.2 Optical Cardiac Monitoring 5

1.3 Microelectrode Arrays 6

1.3.1 High Density MEAs 7

1.3.2 Transparent MEAs 8

1.3.3 Flexible MEAs 10

1.4 Silver Nanowire 10

1.4.1 Transparency 12

1.4.2 Flexibility 14

1.4.3 Electroplating for Biocompatibility 14

Chapter 2: Experimental Methods and Materials 16

2.1 Fabrication 16

2.1.1 PET Film and Substrate 16

2.1.2 Silver Nanowire Deposition 17

2.1.3 Probe Definition with Laser Cutting 20

2.1.4 Encapsulation 20

2.1.5 Gold Electroplating 21

2.2 Microelectrode Characterization 21

2.2.1 Optical Properties 21

2.2.2 Electrochemical and Mechanical Properties 22

Chapter 3: Results and Discussion 25

3.1 Optical Results 25

3.2 Electrochemical and Mechanical Results 27

3.3 Discussion 33

Chapter 4: Future Work **36**
4.1 Further Testing and Characterization 36
4.2 Biotesting 36
4.3 Stretchability 37
4.4 Scaling up Further: 144 Channel Device 38
4.5 Improving Electrode Performance: PEDOT: PSS 40
Chapter 5: Conclusion **41**
References **42**

List of Figures

Figure 1. Diagram of action potential in cardiomyocytes [2] 2

Figure 2. Microelectrode array overlaid on the heart surface [7] 6

Figure 3. GCaMP6 mouse cortex fluorescence images. e) Transparent graphene MEA. f) Opaque platinum MEA [12] 8

Figure 4. A transparent microelectrode array fabricated with a nanogrid structure [7]..... 9

Figure 5. Electrogram waveform captured by 4 silver nanowire electrodes [20]..... 11

Figure 6. Magnified microscope image of a silver nanowire network 12

Figure 7. Silver nanowire based multimodal optoelectronic measurement probe [20] ... 13

Figure 8. Elemental mapping of gold and silver, showing a core-shell structure [20] 15

Figure 9. a-e) Fabrication flow of 64 channel soft MEA..... 16

Figure 10. Silver nanowire film with aggregations..... 18

Figure 11. Transmittance spectra for an unplated silver nanowire film, one plated with gold for 10 seconds, and one plated with gold for 15 seconds 25

Figure 12. Image of transparent MEA placed over a George Washington University logo 26

Figure 13. Nanowire network over a large area film 27

Figure 14. a) Impedance spectra of a pristine silver nanowire electrode, an electrode plated with gold for 10 seconds, and an electrode plated with gold for 15 seconds. b) Phase spectra of the 10 second plated electrode. 28

Figure 15. MEA response to a generated 2 mV peak to peak sine wave..... 29

Figure 16. Change in sheet resistance for various feature widths..... 30

Figure 17. Change in sheet resistance of an unplated and gold-plated film when exposed

to oxygen plasma 31

Figure 18. a) Change in impedance over 5000 bending cycles. b) Optical image showing the flexibility of the device 32

Figure 19. Comparison of our gold-plated silver nanowire and other common transparent, flexible materials 34

Figure 20. Nanowire network behavior when exposed to stretching force [41] 38

Figure 21. (left) 64 channel MEA AutoCAD drawing. (right) 144 channel MEA AutoCAD drawing 39

Chapter 1: Introduction

1.1 Cardiac Disease and the Mechanisms of Heart Function

In 2020, one in three adults in the United States received treatment for a cardiovascular condition, costing nearly $400 billion and solidifying cardiovascular disease (CVD) as the leading cause of death in the US [1]. The American Heart Association expects the medical cost of heart disease treatment to nearly quadruple within the next thirty years, reaching a staggering annual cost of $1490 billion [1]. With epidemiological trends pointing towards a rise in CVD, it is of the utmost importance for researchers and medical professionals to have access to a robust tool set for cardiac study.

An understanding of the tools available for cardiac study requires an understanding of the underlying detectable mechanisms of heart function. Broadly, three measurable phenomena drive the rhythmic beating of the heart: electrical depolarization which initiates the beat and coordinates cardiomyocyte behavior, calcium ion activity which converts the initial electrical impulse into muscle contraction, and metabolic activity which provides the energy required by the former two mechanisms.

The cellular unit of cardiac tissue, the cardiomyocyte, is an excitable cell. This enables the generation of a measurable electrical response when stimulated to a certain threshold voltage. This electrical response follows a rhythmic pattern and is referred to as the cardiac action potential [2].

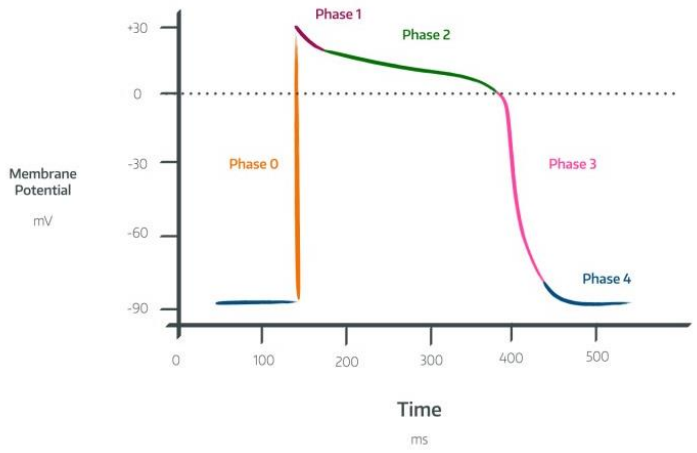

Figure 1. Diagram of action potential in cardiomyocytes [2]

The cardiac action potential begins with cardiomyocytes at rest, a state defined by a membrane potential of around -90 mV [3]. When electrically stimulated past a threshold voltage of around -70 mV, voltage gated ion channels permit the exchange of ions through the cardiomyocyte membrane [3]. Phase 0 of the action potential is driven by the rapid influx of Na^+ ions in atrial and ventricular cells, however in the sinoatrial node, this effect is attributed to Ca^{2+} ion flow [3]. After abrupt depolarization, the relevant voltage sensitive Na^+ ion channels shift into a closed state, while a small number of rapid K^+ ion channels activate, allowing the flow of K^+ out of the cell and reducing the membrane potential to near 0, characteristic of phase 1 [3]. Phase 2 is calcium dependent, with L-type Ca^{2+} ion channels counteracting the efflux of K^+ ions, balancing the membrane potential for several milliseconds. This plateau phase is vital for effective contraction of the heart, as the chambers require sustained depolarization to fully empty themselves of blood [3]. Phase 3 begins when Ca^{2+} ion channels close and K^+ ion channels remain open, returning the heart to phase 4, its resting state with a membrane potential of -90 mV. While the cardiac action potential can be explained in terms of a single cell, in practice it is an organ wide phenomenon. Cardiomyocytes depolarize in waves, with each cell

exciting those near it after the initial impulse is generated in the sinoatrial node by pacemaker cells [3].

This organ wide electrical coordination enables organ wide mechanical coordination through the interactions of Ca^{2+} ions, which bridge the gap between the action potential and cardiomyocyte contraction. This process is referred to as excitation contraction coupling. During phase 2 of the cardiac action potential, a small number of Ca^{2+} ions enter the cardiomyocyte. This small amount of calcium interacts with ryanodine receptors on the sarcoplasmic reticulum, resulting in a much larger amount of calcium to be released from within the cell in a process called calcium induced calcium release [2]. This released calcium interacts with troponin C, eventually allowing actin and myosin filaments to interact, resulting in the contraction of cardiac tissue on a chamber wide level.

Both electrical depolarization and mechanical contraction consume a vast amount of energy, requiring high rates of metabolic activity in cardiomyocytes. Despite its great need for energy, the heart only stores enough for a few beats at a time, indicating highly active metabolic production processes to maintain long term function [5]. Most of the heart's energy is produced by way of oxidative phosphorylation, which reduces NAD^+ to NADH and FAD^+ to $FADH_2$ [5]. Their vital role in the electron transport chain and energy synthesis has made these molecules strong indicators of metabolic activity in cardiac tissue.

1.2 Cardiac Monitoring

Various recording techniques have long been leveraged to observe the mentioned mechanisms of cardiac function. Electrical and optical recording methods I particular have proven useful in observing these mechanisms, although neither method is free of

drawbacks or limitations.

1.2.1 Electrical Cardiac Monitoring

Electrical monitoring methods are widely considered to be the gold standard of cardiac monitoring [2]. The regularity and strength of electrical activity across heart chambers is a fantastic indicator of general heart health and function, and the high temporal resolution of measured electrical signals gives great insight into millisecond-to-millisecond changes in observed tissue. The signal amplitude of widespread cardiac electrical depolarization is high relative to other biosignals and can even be measured from the surface of the skin. This is the working principle of one of the most well-known devices for cardiac monitoring: the electrocardiogram (ECG). While the ECG is a simple, non-invasive method of assessing cardiac health, it does not provide a full summary of the electrical activity of the heart [3]. The ECG is a tool operated on the organ level, and while behavior of the atria can be discerned from the behavior of the ventricles due to signal amplitude differences [3], precise information, such as the speed and shape of electrical signal propagation, is lost.

On a far smaller scale, technology like patch clamp recording can provide insight into the behavior of individual cardiomyocytes and the ion channels that govern their electrical activity [2]. This intracellular recording method is capable of isolating specific areas of the cell membrane using a small pipette, allowing the observation of ion flow through membrane bound channels. While this technique is immensely valuable in providing insight into individual heart cell behavior, it is incapable of recording behavior of heart tissue as a whole. This limits the effectiveness of patch clamp recording techniques in the study of CVD, which demands the study of the heart on a tissue level at minimum.

Overall, electrical monitoring of the heart represents a high temporal resolution view into electrical activity of the heart, but fails to observe cardiac activity on a tissue or chamber scale or provide insight into calcium ion handling or metabolic activity.

1.2.2 Optical Cardiac Monitoring

Optical cardiac monitoring relies upon fluorescence, either of various dyes loaded into the heart, or of autofluorescent molecules already existing in cardiac tissue [4]. The use of dyes allows the observation of elements and metabolic molecules in the heart that are not observable through electrical observation. Optical monitoring also provides remarkable spatial resolution, allowing the observation of small features over wide ranges of the heart.

Calcium sensitive dyes have enabled the observation of calcium transients during excitation contraction coupling of the heart [4]. When these dyes bind to calcium, their optical properties shift, either fluorescing with a higher intensity, or fluorescing at a different wavelength [4]. This allows the observation of when calcium induced calcium release occurs and provides insight into the amount of calcium released during the process, vital for the understanding of various calcium related pathologies that result in CVD.

Certain methods of optical imaging are label-free and do not require dye for imaging. One example is the observation of NADH and FAD^{+}, both of which fluoresce naturally when stimulated at particular wavelengths [5]. This enables the optical study of metabolic behavior in cardiac tissue. The more of each molecule that exists, the stronger the intensity of the fluorescent response, giving an indication of whether metabolic pathways are creating and expending these resources in expected quantities.

While optical monitoring methods produce images with high quality spatial

resolution, their temporal resolution is poor in comparison to electrical monitoring methods. This is due largely to the time it takes for excited fluorescent molecules to return to their ground state, as well as limitations in how quickly photons can be captured [4].

Current research acknowledges that heart disease is a multiparametric issue. Neither optical nor electrical data alone is sufficient in understanding the complex mechanisms that underly the onset and perpetuation of lethal arrhythmias [6]. For this reason, there is great value in the development of tools which allow for simultaneous electrical and optical monitoring of cardiac tissue. This integration permits simultaneous observation of the three vital mechanisms of heart function, producing data with the high temporal resolution of electrical recording and the high spatial resolution of optical recording.

1.3 Microelectrode Arrays

This goal of optoelectronic integration requires an electrical measurement device capable of operating on the same scale as optical imaging techniques. Microelectrode arrays (MEAs) have proven to be a viable option to satisfy this requirement.

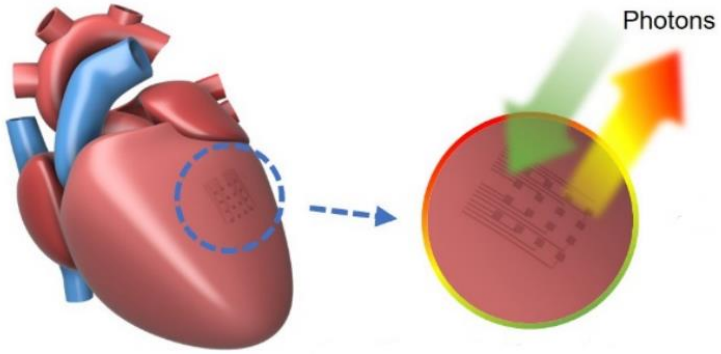

Figure 2. Microelectrode array overlaid on the heart surface [7]

With multiple micro-scale electrodes simultaneously recording at the surface of the heart,

MEAs allow the capture of electrical signal propagation on the tissue, or even chamber level if the MEA large enough. There are several important directives for improving the performance of MEAs for optoelectronic applications in cardiac tissue: Creating higher density MEAs for better spatial resolution, developing transparent MEAs to allow simultaneous optical and electrical recording, and creating MEAs with favorable mechanical properties relative to soft, moving cardiac tissue.

1.3.1 High Density MEAs

The density of microelectrodes in the array is an important metric to consider when determining how effectively an MEA can monitor a particular area. Arrays with large gaps between electrodes are said to have low spatial resolution. Within these gaps between electrodes, cells are unobserved, and any behavioral conclusions made about them must be inferred from populations of cells that are measured [8]. Inference from low spatial resolution is acceptable in some cases, but when attempting to discern the precise electrophysiological behavior, or the complex mechanisms behind it, high spatial resolution is key.

Several issues exist at the intersection between high density arrays and arrays intended to monitor a large area, such as a chamber of the heart. Extremely high spatial resolution has been achieved in CMOS-MEA's, however the sheer cost of manufacturing these devices makes them not suitable for scaling up to a larger target area [8]. CMOS devices are also limited to a small set of materials, making initiatives towards transparency and flexibility difficult [8]. More traditional, cost-effective cleanroom fabrication methods such as wet etching and lift off are financially suitable for fabricating a large area device, but are time consuming.

Laser cutting, while it has a high initial cost, is a quick method for defining high

density arrays with small, micro scale feature sizes. With a provided template, a laser cutter will be able to replicate it accurately as many times as necessary without the time cost of cleanroom fabrication.

1.3.2 Transparent MEAs

Transparent MEAs are a sought after innovation for the sake of achieving co-localized optical and electrical recording, giving a deeper understanding of observed tissue [9] [10]. This enables multiparametric measurement of various mechanisms of heart function with complimenting spatial and temporal resolution.

The integration of optical recording capabilities into traditional MEAs is not a problem free process. Traditional MEAs are typically made from opaque metal such as platinum or gold. While the electrical recording capability of these electrodes is acceptable, they obscure any optical signals that might be measured from the same population of cells the electrode sits on [11].

One way to address this issue is to replace opaque conductive materials with transparent conductive materials in MEA fabrication. A vast array of transparent conductors exist, each with their own set of recording capabilities and mechanical properties.

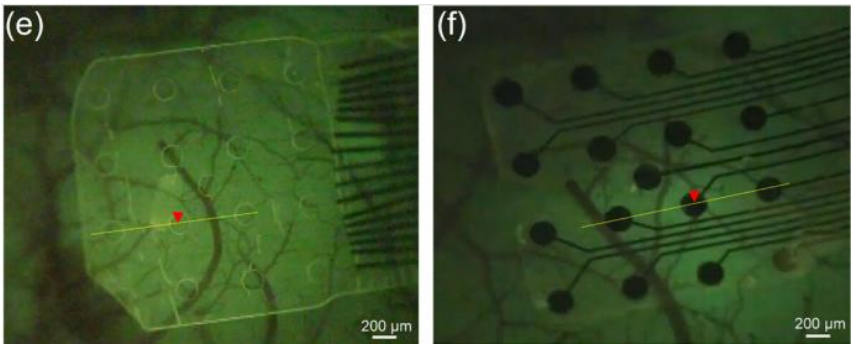

Figure 3. GCaMP6 mouse cortex fluorescence images. e) Transparent graphene MEA. f) Opaque platinum MEA [12]

Figure 3 shows two different types of arrays laid over similar fluorescent tissue. The opaque platinum MEA obscures the tissue it lies over, preventing fluorescent signals from being measured. The graphene MEA, however, allows for a clear picture of the underlying tissue to be taken, allowing for full capture of fluorescent signals. For transparent conductive materials, there is often a tradeoff between transparency and electrical performance [13]. For example, graphene is transparent because it is extremely thin. This thinness lends itself well to optical properties, but is a detriment to the recording capability of the material. Adding thicker layers of graphene will improve electrical performance, but reduce its transparency. A key part in the design process of an MEA utilizing transparent materials is determining where the balance lies between transparency and recording performance.

Opaque conductors may still be used in the creation of transparent MEAs so long as appropriate fabrication techniques are employed. One such strategy is replacing traditional solid metal electrodes with nanogrids made from the same metal [7].

Figure 4. A transparent microelectrode array fabricated with a nanogrid structure [7]

Figure 4 demonstrates how a transparent microelectrode array might be achieved using the metal nanogrid strategy. Instead of a flat sheet of molybdenum serving as the electrode area, molybdenum is instead laid in a grid structure. This shape allows for both

strong electrical recording while also allowing much of the tissue beneath the electrode area to be visible [7]

1.3.3 Flexible MEAs

The heart is a mechanically active organ, constantly in motion. For this reason, the mechanical properties of MEAs meant for cardiac applications are of great concern. Ideally, the mechanical properties of any tissue contacting device should match the properties of tissue, which demands high flexibility from the materials used to ensure biocompatibility [14,15].

As was the case with achieving transparent MEAs, both material choice and fabrication technique can enable the creation of flexible devices. While any number of already well understood polymers such as polyethylene terephthalate (PET) or polydimethylsiloxane (PDMS) [16] can be used as flexible substrates, there is a more limited list of materials that can be used as flexible conductors.

Flexibility has been achieved in many conductors by carefully managing the thickness of the conductor. Graphene, gold, platinum, and many other standard conductors have all proven flexible when made thin [17]. This can also be said for metal nanowire networks which, due to their high length to diameter ratio, are highly flexible [18]. Conductive polymers are also of interest, displaying the inherent flexibility of polymer structure alongside the ability to perform electrical measurements.

1.4 Silver Nanowire

Silver nanowire is an attractive material with desirable optical and mechanical properties. Silver nanowire has entered the fabrication process for several types of electronics such as solar cells and flexible OLEDs due to its fantastic optoelectronic performance and mechanical flexibility [19]. These same properties make it an ideal candidate for

integration into MEAs for optoelectronic recording. What makes silver nanowire such a strong candidate for MEA fabrication is its solution-based processing ability. Unlike other transparent conductors that may have costly or time intensive deposition processes, silver nanowire is simple to spin coat over a large film, allowing uniform deposition and enabling high density patterning [19]. The ability to perform well over a large film area enables silver nanowire MEAs to measure cardiac activity on a tissue, or even chamber level.

Silver nanowire is most commonly created using polyol synthesis. Adjusting the parameters of this process allows for nanowires of different diameters and lengths to be created [20]. This process is well developed and greatly tunable, ensuring that silver nanowire is simple to obtain in many different aspect ratios for different use cases.

Most importantly to its application in cardiac MEAs, silver nanowire based electrodes have proven capable of capturing the electrogram waveform with high fidelity in previous studies [20].

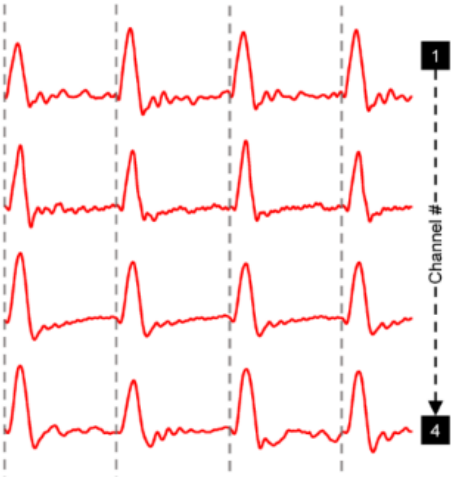

Figure 5. Electrogram waveform captured by 4 silver nanowire electrodes [20]

Effectively capturing the characteristic electrogram signal is highly dependent on an electrode's ability to perform well across a range of biologically relevant frequencies [6]. The electrogram signal itself is comprised of a range of features at varying frequencies. Most features of the human electrogram waveform occur at low frequencies, within the band of .5 – 150 Hz, however studies have shown that higher frequency artifacts indicative of disease may occur in 700 – 1000 Hz bands [6]. Observation of both healthy and disease indicative features of the electrogram waveform is vital to any device which serves as a tool for disease study, meaning that effective silver nanowire electrodes should demonstrate strong electrical recording capabilities within these ranges. Electrical recording capability at particular frequencies is commonly determined through impedance measurements, and frequency bands of cardiac focus will be used to contextualize later impedance results.

1.4.1 Transparency

When silver nanowire is applied to a film, it naturally lays in a random network of crossing wires, as is shown in Figure 6.

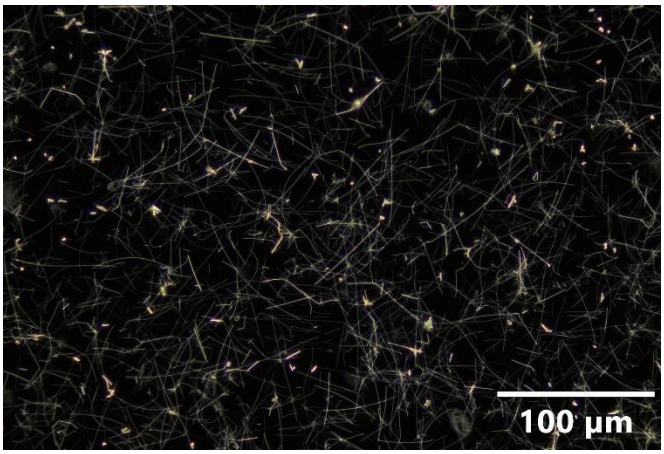

Figure 6. Magnified microscope image of a silver nanowire network

The silver nanowires cross at several points, creating an electrical connection and giving

the film the ability to measure electrical activity. Where nanowires do not lay, light is able to pass through freely, resulting in optical transparency. The degree of transparency will determine both the electrical performance and the transmittance of the nanowire [21]. A higher concentration of nanowire will lead to the creation of a more robust network and a greater number of intersections between wires, but leave fewer empty spaces for light to pass through. Depending on the desired application of the device, this balance between electrical and optical performance can be adjusted as desired.

The transparency of silver nanowire lends itself well to robust optical applications. Below is an example of a multimodal measurement probe that utilizes the transparency of silver nanowire to enable simultaneous optical and electrical measurement and stimulation (Figure 7) [20].

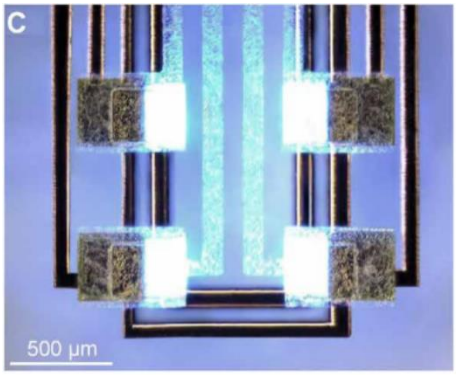

Figure 7. Silver nanowire based multimodal optoelectronic measurement probe [20]

This device is a 2 x 2 array, featuring four silver nanowire electrodes, each placed on top of a micro photodetector and micro-LED. The monolithic fabrication strategy of this device allows for optical and electrical recording of the same populations of cells simultaneously [20], displaying the favorable optical properties of silver nanowire as a transparent conductor.

1.4.2 Flexibility

Silver nanowires are naturally flexible due to their high aspect ratio [22]. Their small size and elongated geometry demonstrate immense potential for flexibility while still maintaining electrical contact with the surrounding network. While several other transparent conductors like graphene and ITO are also flexible due to their thinness, they are often not flexible enough for cardiac applications. These materials meet the lesser flexibility requirements of neural applications, but when bent around the comparatively aggressive curvature of the heart, they will deform and suffer a loss in electrical performance [12]. Silver nanowire exhibits a markedly higher level of flexibility than other transparent conductors, making it an optimal candidate for cardiac applications.

1.4.3 Electroplating for Biocompatibility

Studies have observed that silver nanowire, when left in contact with tissue, causes a wide variety of cytotoxic events [23]. This makes any device with silver nanowire electrodes that contact the biofluid unsuitable for long term monitoring and not truly biocompatible. In addition, any silver in long term contact with biofluid will oxidize, reducing the electrical performance of the electrode and shortening the device's lifespan. A common strategy used to improve the biocompatibility of silver nanowire and protect it from oxidation is to electroplate the network with gold, an inert metal that does not react with biofluid and demonstrates strong electrical measurement capabilities. Typically, a film with exposed silver nanowire is placed into a solution with dissolved gold ions from gold salts. A current is then run through the nanowire, chemically adhering gold wherever there is conductive silver through a reduction reaction which converts suspended gold ions into solid gold.

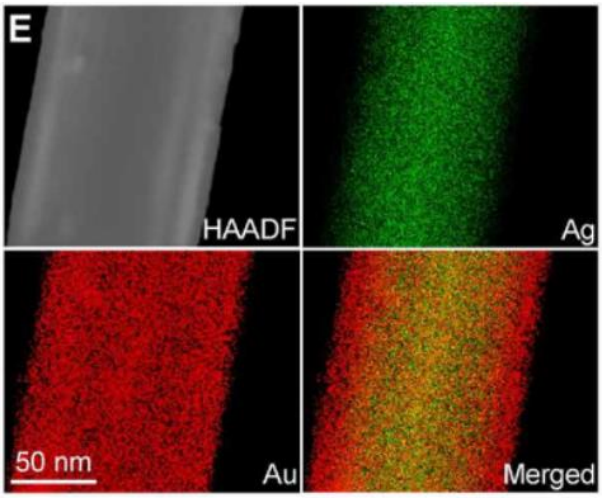

Figure 8. Elemental mapping of gold and silver, showing a core-shell structure [20]

The result of the electroplating process can be seen in Figure 8 which uses an energy dispersive spectroscopy technique to determine the structure of a silver wire (green) plated with gold (red). The merged image shows a distinct shell around the silver core, meaning that there is no longer exposed silver, thus no threat of cytotoxicity or oxidation for gold plated silver nanowire.

Again, a tradeoff is encountered. While plating silver with gold is necessary to ensure biocompatibility and device longevity, the thickness of the shell around the silver core can impact transmittance. Thicker shells lead to better insulated silver, but a less transparent film overall.

Chapter 2: Experimental Methods and Materials

In this chapter, the fabrication process for a high density, 64 channel, flexible, silver nanowire-based microelectrode array is discussed. In addition to the materials and processes used, experimental procedures for optical and electrochemical performance tests are described.

2.1 Fabrication

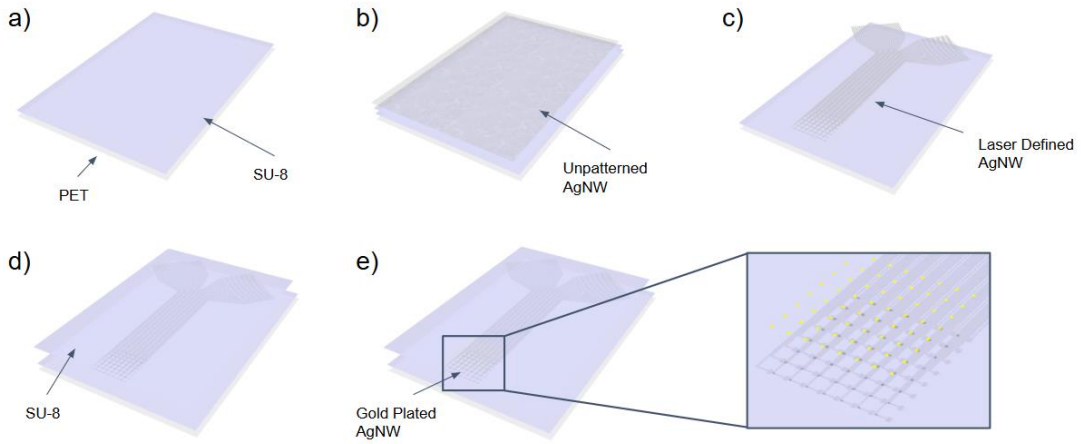

Figure 9. a-e) Fabrication flow of 64 channel soft MEA

2.1.1 PET Film and Substrate

The fabrication process shown in Figure 9 begins with laminating a PET film onto a glass slide, which serves as a handling substrate. While much consideration has been given to the optical and mechanical properties of silver nanowire, that effort would mean little if the substrate the conductor was patterned on did not also exhibit the same optical and mechanical properties. PET is transparent and can be purchased in many different thicknesses, with thinner PET being more flexible, but more difficult to laminate uniformly, introducing the possibility of defects on the patterning surface. A balance between flexibility and ease of handling was found with 8 µm thick PET.

PDMS was spin coated onto the glass handling substrate to serve as an adhesive layer between it and the PET film, providing a surface that the PET film can adhere to for the duration of the fabrication process and be removed from later. This strategy allows the PET film with the conductor patterned on top to be peeled off and seamlessly separated from the handling substrate when the fabrication process is complete.

A 0.5 μm thick SU-8 2000.5 (MicroChem, Westborough, MA) adhesive layer was spin coated on top of this layer to serve as both a planarization layer and adhesive layer for silver nanowire. The purpose of a planarization layer is to ensure that the surface of the device is as smooth as possible for later fabrication steps, ensuring even distribution of nanowire and reducing the possibility of mechanical defects diminishing the performance of the device. SU-8 also serves as a substrate that nanowire can embed into, giving greater mechanical stability to the device and anchoring the nanowire onto the substrate.

In addition to properties such as transparency and flexibility, each substrate was also selected for its ability to withstand the remainder of the fabrication process. PDMS, PET, and SU-8 all display suitable heat and chemical resistances to meet this need.

2.1.2 Silver Nanowire Deposition

Silver nanowire of 20 μg/mL initial concentration was purchased from ACS Materials (Pasadena, CA, USA). Silver nanowire purchased in this manner comes as a highly concentrated suspension of nanowire in isopropyl alcohol. Varying lengths and diameters of nanowire are available for purchase, but for this device, the expected nanowire length used is 55 – 75 μm. Choosing lower aspect ratio nanowires will decrease the likelihood of nanowire aggregations and improve surface uniformity, but it may be difficult for a

robust network to form, as shorter wires will overlap less often than longer nanowires. On the other hand, longer nanowires are more likely to have multiple different connections with other nanowires, leading to a strong electrical network, but large aggregations may be impossible to separate without damage to the wires. 55 – 75 µm was found to be a usable middle ground which allows for uniform distribution and the creation of a robust network.

The initial concentration of nanowire in the stock bottle is far too high to maintain optical transparency. For this reason, before use, the nanowire solution was diluted to 3.5 µg/mL using isopropyl alcohol. This concentration is enough nanowire to form a network, but not so much that the nanowire network obscures light.

A significant issue that may be encountered when working with silver nanowire is nanowire aggregation, as pictured in Figure 10.

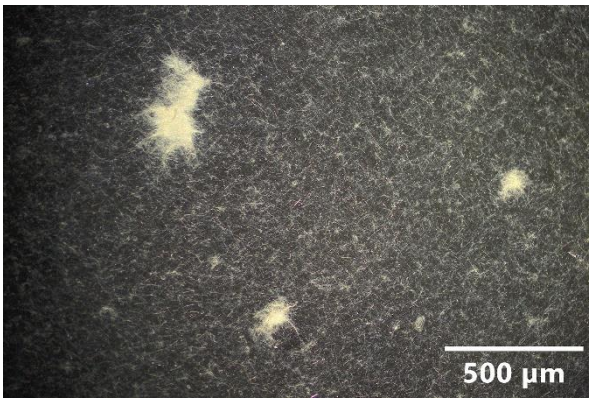

Figure 10. Silver nanowire film with aggregations

These nanowire aggregations are problematic for two main reasons. First, nanowires locked up in clusters do not contribute to the robustness of the overall network, reducing the electrical performance of the film. Second, large, opaque objects in the film reduce its overall transmittance.

There are several strategies that can be used when handling silver nanowire to

prevent the formation of aggregations. One is ultrasonication, which is a common strategy used to break up and disperse nanoparticles. Ultrasonication applies high frequency noise as a method of physical agitation. This strategy can be effective to a degree where silver nanowire is concerned, but must be applied in moderation, as excessive sonication may break nanowire [24], reducing the electrical conductivity of the network. Another method of separating aggregations is chemical treatment, specifically with zwitterionic surfactants. Zwitterionic surfactants consist of dipole molecules. When applied to silver nanowire, the anionic end of the molecule absorbs onto the surface of the wire, leaving the cationic ends to repel each other, effectively pushing the nanowire aggregations apart without fracturing individual wires [25]. Both strategies help to ensure uniform nanowire distribution across a film, increasing the reliability and percent yield of the fabrication process and reducing the negative impacts of random nanowire network formation.

In the fabrication of this device, both Zwitterionic surfactants and ultrasonication were used to break up nanowire aggregations. First, diluted nanowire was left to sit in zwitterionic surfactant overnight, utilizing ionic interactions between wires to gently push them apart. Before use, the nanowire was centrifuged and washed thoroughly several times to ensure that no surfactant remained on the wires. Second, prepared nanowire was vortexed and ultrasonicated for 100 seconds twice. This mechanical agitation process served to break up smaller, less complex aggregations that may have formed from the nanowire settling in the solution or from the washing process.

Prepared nanowire was distributed onto the film using a spin coater. This method allows us control over the speed and acceleration of rotation in distribution. Slower

speeds will allow the nanowires greater opportunity to anchor themselves onto the film, but will also allow aggregations to form. In order to improve the robustness of the nanowire network, the spin coating process used to distribute nanowire on the film was done twice. This allows the second dispersion of nanowire to catch and anchor on the rough texture of the first, resulting in more opportunities for electrical connection across the film.

2.1.3 Probe Definition with Laser Cutting

We used an LPKF U4 laser cutter to define the nanowire pattern seen in section c of Figure 8. The laser cutting pattern was generated in AutoCAD then loaded into the laser cutter for processing. In this pattern, electrodes are placed 500 microns apart, achieving high spatial resolution relative to current standards [26]. Not pictured in Figure 8 is a mesh structure cut out of the large, non-functional areas of the film, such as between electrodes and around the edges of the device. The mesh cut out within the array serves to allow biofluid flow around electrodes, as depriving tissue below the array of necessary nutrients may result in abnormalities in heart behavior. The mesh cut out around the array area is intended to allow easy securing of the device via pins to facilitate biotest set up. This is especially useful for small heart models with more aggressive curvatures than larger hearts which would allow the device to lay directly on it without such deliberate fastening.

2.1.4 Encapsulation

In order to ensure that only the electrode surfaces contact the biofluid, encapsulation is necessary. To achieve this, a 7 μm thick SU-8 2007 was spin coated on the device, and the entire film except for 64 250 X 250 μm electrode areas were exposed to UV light, curing the photoresist. This electrode window size has proven sufficient in past cardiac

studies [23]. The device was then baked at 110 °C, allowing the SU-8 that had been exposed to UV light to fully crosslink, solidifying it on the device and making it unremovable. Unexposed resist was removed with SU-8 developer, leaving open windows over the electrodes allowing biofluid contact.

2.1.5 Gold Electroplating

The electroplating process begins with placing the encapsulated device into a sulfite-based gold salt solution which has been heated to 60°C (TSG-250, Transene). Before use, this solution is diluted with deionized water at a 1:8 volume ratio. In order to assess the relationship between impedance and transmittance at varying gold plating thicknesses, devices were made unplated, with 10 seconds of plating time, and with 15 seconds of plating time. Plating was performed using a potentiostat (Reference 600+, Gamry Instruments Inc.) with a three-electrode configuration. A saturated Ag/AgCl electrode served as the reference electrode, a platinum wire served as the working electrode, and the device itself served as the counter electrode. A current density of 0.1 mA/cm² was administered to plate the gold ions onto the bare silver nanowire. The application of current reduces suspended gold ions, resulting in the creation of solid gold on the surface of any conductive silver in a thin, uniform layer. After electroplating, the device was washed thoroughly with deionized water to remove remaining debris and residue.

2.2 Microelectrode Characterization

2.2.1 Optical Properties

The transmittance spectrum of the device was obtained using a spectrophotometer (V-770, Jasco, Inc.). The nanowire transmittance spectrum was obtained over a range of wavelengths from 400 nm to 800 nm, as these wavelengths are most relevant to cardiac fluorescent imaging [27].

Since this model of spectrophotometer was designed to hold cuvettes, this experiment was done with a large film rather than a single electrode to ensure that the nanowire spanned the entire measurement area. The fabrication process of this film is identical to a functional device, but with no laser patterning step. In order to ensure that only the transmittance and optical artifacts of the nanowire network was being analyzed, a reference film of PET and SU-8 was used during measurements. This experiment was repeated three times, one with bare silver nanowire, one with 10 seconds of gold plating, and another with 15 seconds of gold plating. As gold plating time increases, we expect to see the transmittance across the range of wavelengths decrease, as the thicker diameter of the heavily plated nanowires will obscure more light.

2.2.2 Electrochemical and Mechanical Properties

Electrochemical impedance spectroscopy (EIS) was used to obtain the impedance and phase spectra of patterned electrodes. Measurements were made with a potentiostat (Reference 600+, Gamry Instruments Inc.) using a three-electrode configuration. For EIS measurements, a saturated Ag/AgCl electrode served as the reference electrode, a platinum wire served as the counter electrode, and the patterned electrodes of the MEA served as the working electrode. Measurements spanned from 1 - 100,000Hz with a scan rate of 100mV/s. Like transmittance, this test was performed with electrodes gold plated at various durations. As plating time increases, we expect to see a decrease in the amplitude of the impedance spectra, indicating stronger recording capabilities. Both tests were performed in a phosphate buffered saline (PBS) solution (Sigma Aldrich) diluted 10:1 with deionized water.

In order to test the recording fidelity and resolution of a plated electrode, an experiment was performed to determine if there was significant signal loss while

measuring a changing, distinctly shaped signal. If functioning optimally, the device will be able to return this signal with minimal loss in amplitude and no distortion of shape. A PowerLab data acquisition system (ADInstruments Inc.) was used to generate a 2 mV peak to peak sine wave in PBS solution. The device was placed into this PBS solution to measure the generated sine wave. The measured wave was extracted for review using LabChart software.

The reliability of silver nanowire networks as conductors was analyzed at various feature sizes. It can be assumed that solid metal, so long as it is not broken, will remain conductive at extremely small feature sizes. This cannot be assumed for silver nanowire, as there is no guarantee that the nanowire network will contain overlapping nanowires within narrow features. To assess the limit of feature sizes, a nanowire film was laser cut with features of various sizes ranging from 50 µm to 250 µm in width. A four-point probe (SRM-232, Guardian Manufacturing Inc.) and source meter (2614B, Keithley) were used to generate IV curves for each feature size in LabView software. From this IV curve, sheet resistance was determined for each feature, and the change in sheet resistance based on feature size was analyzed. Reliable performance at small feature sizes would demonstrate silver nanowire's ability to function as a conductor in high density patterns.

To verify the effectiveness of the gold electroplating procedure, a gold-plated film's capacity to oxidize was measured against an unplated film. The resistance across both films was measured with a multimeter before oxidation to establish a baseline resistance. Both films were then placed into an oxygen plasma cleaner (PDC-001-HP, Harrick Plasma) on high power for 2 minute intervals up to 6 minutes. Exposure to

oxygen in this manner will oxidize any exposed silver, while leaving gold unaffected. If the silver of the plated film is completely encapsulated by gold, then the resistance of the network should not change.

The flexibility of the device was assessed using a motorized test stand (ESM 1500, Mark-10). A device was measured for its baseline impedance at 1k Hz, then bent around a 5 mm radius for 5000 total bending cycles. The device's impedance was measured at 1000 cycle intervals. If the device is able to withstand mechanical bending, then the impedance of the device should not change from the baseline value despite undergoing several thousand bending cycles.

Chapter 3: Results and Discussion

3.1 Optical Results

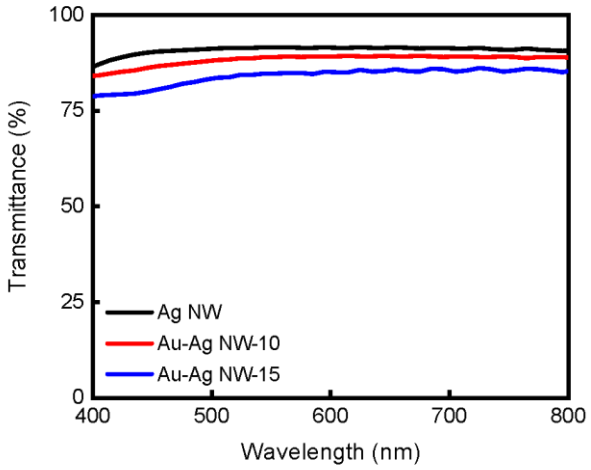

Figure 11. Transmittance spectra for an unplated silver nanowire film, one plated with gold for 10 seconds, and one plated with gold for 15 seconds

Figure 11 shows the transmittance results for three films prepared at various gold plating conditions. The unplated film, the film plated for 10 seconds, and the film plated for 15 seconds achieved average transmittances of 91.0%, 88.5%, and 84.4% respectively. As expected, as the duration of gold plating increases, the shell of gold around the silver nanowire core becomes thicker and the transmittance of the film decreases. Despite this, all three films exhibit competitive transmittance values near the 85% - 95% range seen in recent literature [28-30]. The device also performs well optically at several wavelengths relevant to optical cardiac imaging. For calcium imaging, the excitation wavelength is around 470 nm, and the emission wavelength is around 520 nm [31]. At 470 nm, the unplated, 10 second plated, and 15 second plated films achieve 91.1%, 87.8% and 83.15% transmittance respectively. At 520 nm they achieve 91.6%, 88.9% and 84.7%

transmittance. These results indicate strong potential for integration into calcium imaging techniques, as the vast majority of signal remains measurable.

Figure 12. Image of transparent MEA placed over a George Washington University logo

Figure 12 demonstrates the visual transparency of the device with the George Washington University logo clearly visible from underneath the array. This image demonstrates that the transparency of the device is not limited to the electrode area, enabling greater view of the tissue beneath it in cardiac applications.

Another important facet of optical transparency of silver nanowire is the quality and uniform distribution of the nanowire network. Aggregations can be a great detriment to the overall transmittance of a film and disturb the transmittance spectrum with optical artifacts that cannot be explained by the normal properties of silver nanowire. Figure 13 shows an image of the achieved nanowire network taken under a microscope.

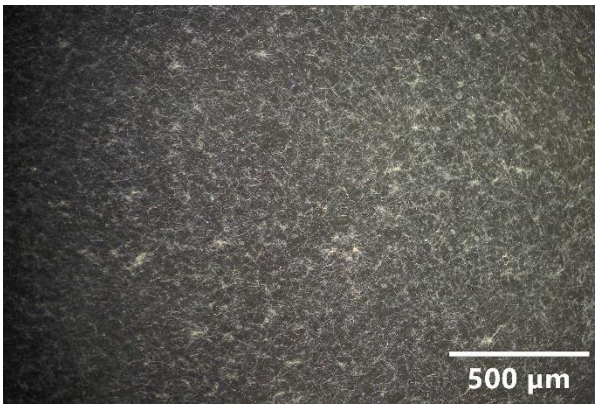

Figure 13. Nanowire network over a large area film

There is strong uniformity of the nanowire network over the film observed. While some areas of aggregation do exist, they are small and not entirely opaque, indicating the effectiveness of ultrasonication and zwitterionic solutions as tools for ensuring uniform silver nanowire dispersion. Improving the uniformity of this network further is an initiative that deserves effort, as the dissolution of these remaining areas of aggregation will only serve to improve overall transmittance.

3.2 Electrochemical and Mechanical Results

The most basic metric for the performance ability of an electrode is its electrochemical impedance. A low impedance will lend itself to a high signal to noise ratio, allowing precise capturing of electrical biosignals.

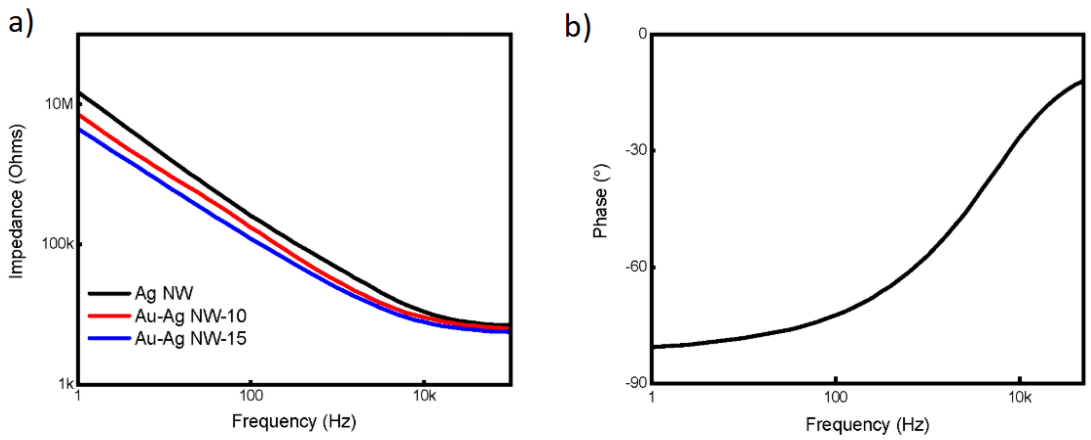

Figure 14. a) Impedance spectra of a pristine silver nanowire electrode, an electrode plated with gold for 10 seconds, and an electrode plated with gold for 15 seconds. b) Phase spectra of the 10 second plated electrode.

Figure 14.a verifies the assumption that an increase in gold plating time increases electrical performance ability; as the plating time increases from 0 seconds to 10 seconds to 15 seconds, the measured impedance decreases over the full range of 1 - 100,000 Hz with no intersection between curves. The decrease in impedance as the thickness of the gold shell increases can be attributed largely to an increase in the functional surface area of the nanowire network [32]. This increase in surface area decreases the resistance of the electrode, leading to stronger electrical recording capability. While this improvement remains observable across the entire scanned frequency range, special attention must be paid to the measurements taken at 1 kHz. The frequency range of 0.5 - 1,000 Hz is known to be vital for biological recordings [33]. Thus, the best conclusion about the electrical performance of the device can be drawn from measurements in that range. At 1 kHz, impedance decreases from 46.3 kΩ to 29.5 kΩ to 25 kΩ. Though the smallest impedance is observed in the electrodes gold plated for 15 seconds, they also display the worst

optical properties out of the three tested conditions. Likewise, an unplated electrode displays the best transmittance observed alongside the highest impedance. For the sake of balancing the tradeoff between optical and electrical performance, the electroplating duration will be set to 10 seconds for future figures.

Figure 14.b shows the phase plot of the gold-plated silver nanowire. As frequency increases, the phase shifts from -80.6° at the lowest frequencies to -12° at the highest frequencies. The phase angle of the lower range indicates capacitive behavior, while the phase angle of the higher range indicates resistive behavior [34]. This capacitive behavior in low frequency ranges is ideal for the application of the MEA, in which it should be able to observe electrochemical changes but not respond to or influence them [34].

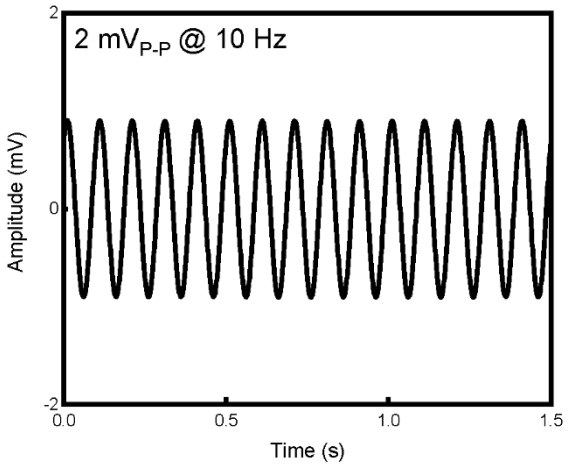

Figure 15. MEA response to a generated 2 mV peak to peak sine wave

The low impedance of the gold-plated electrodes bodes well for its electrochemical recording capability. To further verify the device's recording capability, the MEA was exposed to a 2 mV peak to peak sine wave, a waveform with a distinct shape and known amplitude at all points. If the device's electrical recording fidelity is high, the output signal should match the input sine wave with no distortions or significant loss in

amplitude. Figure 15 shows the output signal measured by the MEA over a period of 1.5 seconds. The measured sine wave shows no significant amplitude decrease from the expected 1 mV and -1 mV peaks, indicating low signal loss. Moreover, there are no visible distortions to the expected shape of the measured waveform, indicating recording stability and a resistance to noise interference.

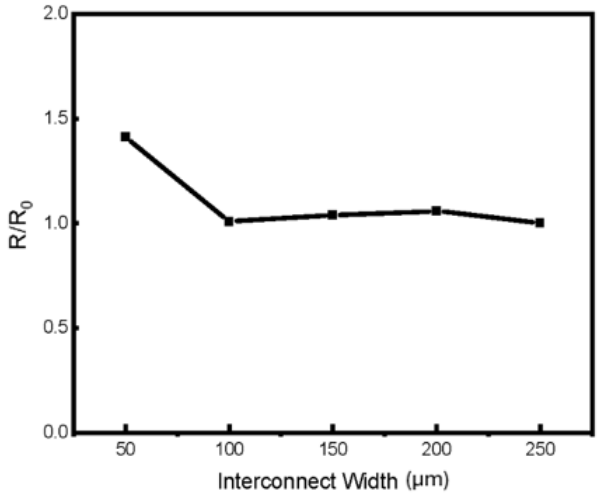

Figure 16. Change in sheet resistance for various feature widths

One of the most straightforward ways to improve the spatial resolution of an MEA is to reduce the sizes of the features of the device, including electrodes and the interconnects that link them to measuring boards. That is, increase the density of MEA patterns. The greatest consequence of this strategy is the increase in impedance that may come with reduced feature size. In order to ensure that the electrical capabilities of the MEA did not suffer from our efforts to minimize feature sizes and increase density, changes in sheet resistance were analyzed over various feature widths. This experiment focused on the smallest feature of the device, the interconnects, which are 100 μm in width. 100 μm width interconnects show no significant difference in sheet resistance when compared with interconnects as large as 250 μm. However, when interconnects become smaller

than 100 µm, sheet resistance does increase, indicating a drop in electrical performance. The 100 µm width interconnects used in the MEA represent the smallest possible interconnect width without decline in measuring capabilities. Further optimization of the nanowire distribution process across the film may allow for interconnects smaller than this to perform similarly. As it stands, this figure demonstrates silver nanowire's ability to serve as a reliable conductor in high density MEA patterns.

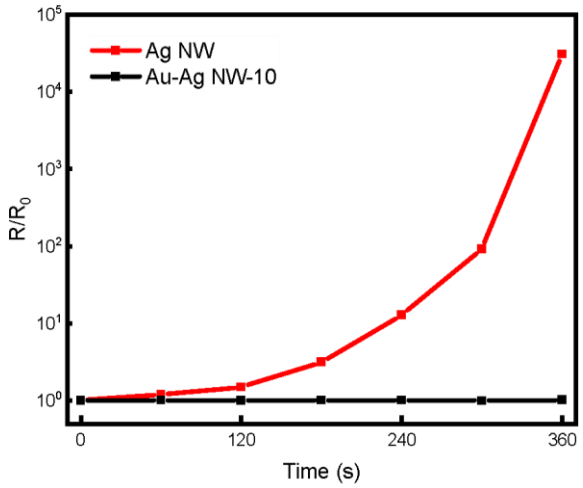

Figure 17. Change in sheet resistance of an unplated and gold-plated film when exposed to oxygen plasma

Transmittance is not the only factor important in the decision of how long to electroplate film. The purpose of gold plating is twofold. One objective is to improve the biocompatibility of silver-based electrodes, preventing silver absorbance by cells interfering with measurements taken. The other is to prevent oxidation of silver by encapsulating it with a non-oxidizable material. To achieve full biocompatibility and stability in this respect, the silver nanowires must not be exposed to the biofluid, demanding full gold coverage. Electroplating for longer times will guarantee the full encapsulation of the nanowires, however this does come at the cost of a decrease in

transmittance. As was the case for impedance, a balance must be found which ensures proper electrical performance, but does not sacrifice optical performance. In order to verify that the gold plating technique used results in fully encapsulated silver nanowire, both an unplated and plated film were oxidized by exposure to oxygen plasma. Sheet resistance measurements were taken for both films, as oxidation will sharply increase the resistance of silver. As expected, the gold-plated film shows no change in sheet resistance over the 6 minutes trial period, indicating reliable gold coverage. On the other hand, the unplated film begins to undergo changes in sheet resistance within the 2 minutes of oxygen plasma treatment. This increase in resistance continues until near non-conductivity at the end of the experiment, further emphasizing the completeness of the gold coverage of the plated film, which prevents its resistance from increasing at all.

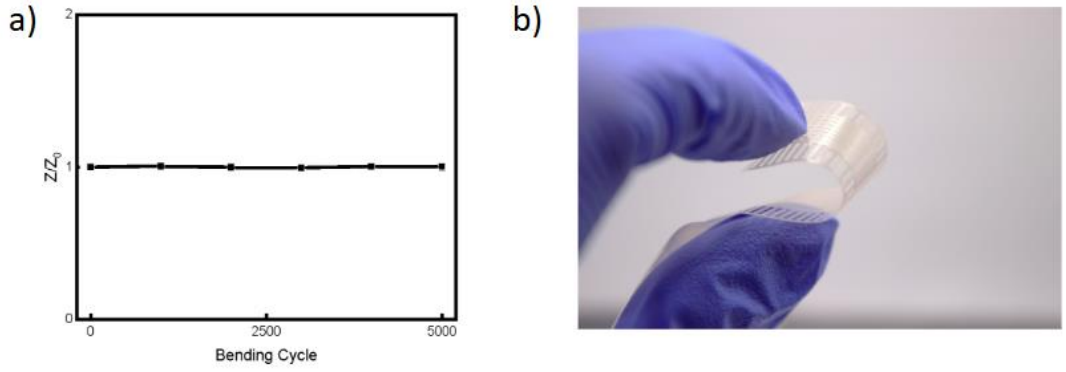

Figure 18. a) Change in impedance over 5000 bending cycles. b) Optical image showing the flexibility of the device

Another facet of biocompatibility for an MEA is its mechanical properties. Ideally, an MEA should be able to sit on the surface of mobile tissue, such as the heart, and retain its electrical recording capabilities despite regular bending. The ability to withstand bending and bending is vital for applying the device in an in vivo or ex vivo study. To assess the

device's resistance to mechanical strain, it was bent around a radius of 5 mm, a curvature relevant to the structure of a rat heart [35], for 5000 total cycles. From 0 to 5000 bending cycles, Figure 18.a shows no significant change in the impedance of the device, indicating a strong resistance to degradation under mechanical strain. This superior mechanical performance is to be expected and attributed to the hyper-flexible materials used in fabrication. Figure 18.b shows the device itself in a bent state, demonstrating its mechanical flexibility.

3.3 Discussion

The characterization results of the proposed 64 channel MEA show strong performance and advancement in all defined target areas. The electrical performance of the device is well within biological measurement standards despite its small interconnect sizes and large area. This electrical performance was achieved while maintaining competitive transmittance results, allowing for the integration of co-localized optical and electrical recording. Long duration mechanical bending tests were unable to damage the device and decrease its performance, indicating feasibility for long term use. Long term use is also ensured by the effectiveness of the gold electroplating strategy, insulating silver from tissue, preventing damage to both oxidation of electrodes and toxicity to the tissue.

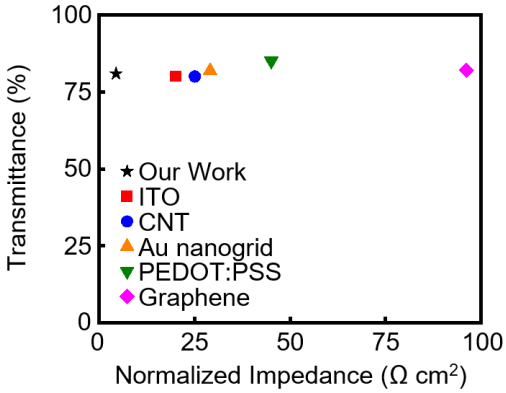

Figure 19. Comparison of our gold-plated silver nanowire and other common transparent, flexible materials

Figure 19 shows a comparison between the normalized impedance and transmittance of the gold-plated nanowire network achieved in this work against other common transparent conductors: Indium tin oxide [36], carbon nanotubes [37], gold nanogrid [38], PEDOT:PSS [39], and graphene [40]. In this figure, impedance is normalized across all materials based on area. This is because larger functional areas naturally decrease the impedance of a material; to ensure fair comparison, all materials must be assessed as if they shared a single electrode size. The transmittance of this device remains competitive with a wide range of other state of the art materials and outperforms them in terms of normalized impedance. This comparison, as well as high achievement in categories of biocompatibility, mechanical flexibility, and recording fidelity solidify silver nanowire as one of the most promising novel materials for cardiac MEA fabrication. Moreover, nanowire is relatively cost effective and is purchasable in several aspect ratios, reducing barriers to entry and providing opportunity for wide scale integration into standard practice. Overall, this design demonstrates a simple, reliable approach for creating highly flexible, highly transparent, high density microelectrode arrays for cardiac monitoring,

capable of achieving co-localized optoelectronic recording.

Chapter 4: Future Work

4.1 Further Testing and Characterization

More benchtop measurements would be valuable in further characterizing the properties of the device. One such test is Cyclic Voltammetry (CV), which could provide further insight into the device's ability to stimulate as well as record through investigation of electron mechanisms.

Optical measurements would also be of great use. Further studies based on the transmittance of light at fluorescently relevant wavelengths would better demonstrate the MEA's potential for optical integration. These tests would involve shining light of specific wavelengths through the device and measuring the irradiance of the resulting signal. Ideally, there should be no significant decrease in measured irradiance, and no distortion of the measured signal as a product of optical artifacts. Wavelengths of focus would include 520 nm and 470 nm relevant to calcium imaging, 460 nm and 360 nm relevant to NADH imaging, and 450 nm to 525 nm relevant to FAD^{+} imaging [31].

4.2 Biotesting

Once benchtop measurements have been completed, the next step for the assessment of any biological measurement device is ex vivo biological demonstrations. While the impedance and recording fidelity of the device are strong, a biotest offers a more dynamic, less controlled testing environment. It would be valuable to verify that the device can perform well despite motion artifacts and conformity to a curved surface. Previous studies have shown that silver nanowire performs well in biological environments [22], but the devices in those studies used a comparatively small number of channels relative to the 64 that would be simultaneously recording in this device. The

most valuable figure to be gained from this study would be a moving map of an electrical signal travelling under the MEA, showing that the MEA is capable of operation on a large scale.

Other studies might involve the addition of drugs to the heart to measure various pathologies. Vasodilators like adenosine may be introduced to observe tachycardia, or ion channel blockers like barium chloride may be introduced to observe arrhythmias. There is also great potential for optoelectronic studies in a biotest setting. This would require a dye to perfuse into the heart, if necessary, a stimulating LED, and a high-speed recording camera to capture generated optical signals.

There is also an opportunity to verify the device's ability to function as a pacer during biological demonstrations. This would be achieved by disconnecting a channel of the device from recording hardware and connecting it to a voltage source. Verifying the device's ability to both stimulate and record cardiac tissue would qualify it as a closed loop system, capable of stimulating as needed relative to the signals it measures.

4.3 Stretchability

One remarkable property of silver nanowire is that its network is stretchable in addition to being flexible. In order for a material to be considered stretchable, it must be able to withstand at least 10% strain relative to the initial length of the material on a substrate [41]. When silver nanowires are deposited on a film, individual wires overlap, creating long chains of electrical conductivity in the network. These overlapping wires do not adhere to each other, making them able to slide and move in compliance with any strain the film undergoes [41]. So long as the wires are not stretched to the point where they are fully isolated from each other, the nanowire network will remain conductive.

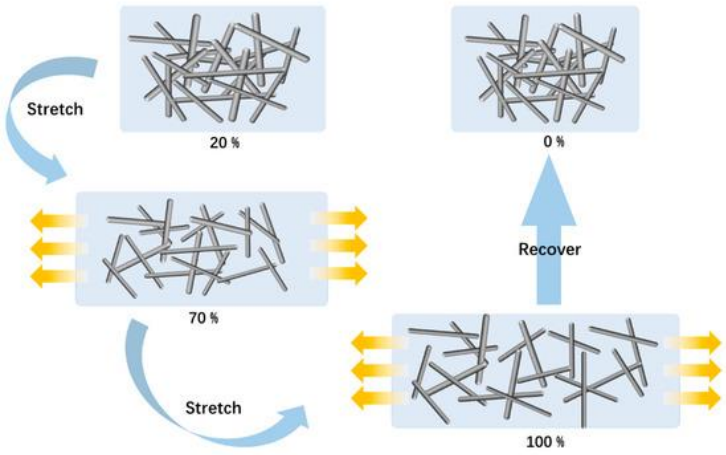

Figure 20. Nanowire network behavior when exposed to stretching force [41]

Figure 20 shows the behavior of nanowires under strain. As they move away from each other, they remain in contact, allowing for the propagation of electrical signals across the film. At extreme levels of stretch, nanowires lose physical contact with each other, reducing electrical performance. The point at which this occurs will determine the stretch tolerance of the device. Another advantage of silver nanowire is that it has great potential for recovery after stretching [41]. After the stretching force is removed, materials may be deformed or have difficulty reverting to their original shape [41]. Silver nanowire networks do not suffer from this difficulty, with individual nanowires simply sliding back into place as the film returns to its original shape. This reduces the impact that stretch has on the overall condition of a device, lending itself to reliable long-term performance. Since this MEA is silver nanowire based, when this fabrication process is reproduced on an elastomer substrate like PDMS, a fully stretchable device could be created. This would greatly increase the biocompatibility of the device, allowing in vivo biotests to occur with minimal mechanical damage dealt to surrounding tissue.

4.4 Scaling up Further: 144 Channel Device

One facet of this design process that warrants further investigation is the use of the laser

cutter for silver nanowire definition. During the course of development, increasing the silver nanowire electrode count to 64 channels from our previous 4 channel work presented immense difficulty. Reliance on traditional cleanroom fabrication methods proved too time consuming to be sustainable. Moreover, changes to the features of the device were difficult to make quickly, as new shadow masks for photolithography would have to be designed then ordered for each change.

When silver nanowire is defined using the laser cutter, however, these issues can be avoided entirely. There is effectively no difference in using the laser to cut a 4 channel, 64, channel or 144 channel devices, so long as an AutoCAD template, shown in Figure 21, can be created.

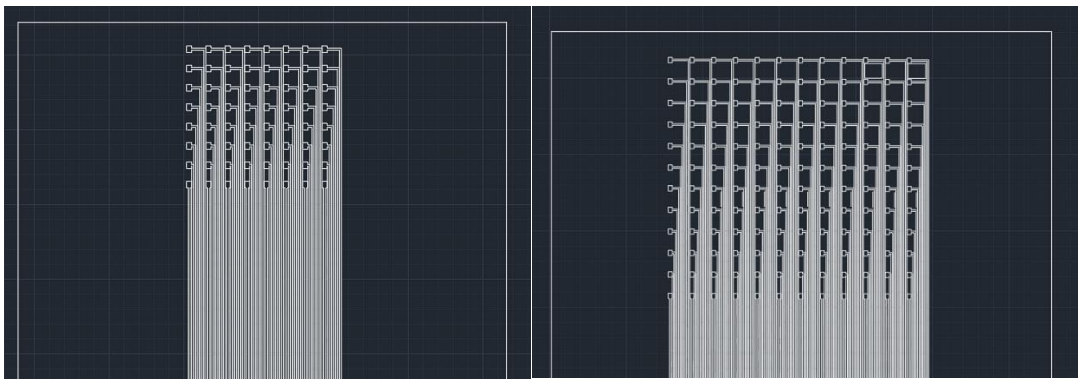

Figure 21. (left) 64 channel MEA AutoCAD drawing. (right) 144 channel MEA AutoCAD drawing

The process for defining the 144 channel array will be no different than the 64 channel array using the laser cutter; where fine tuning a cleanroom fabrication flow may take months with this sort of increase in film area, fine tuning laser cutter protocol will take only a few days. This represents an incredible capacity for fabricating arrays with greater channel numbers, allowing mapping of larger areas of the heart and application to larger heart models.

4.5 Improving Electrode Performance: PEDOT: PSS

The electrical performance of the silver nanowire electrodes, while good, can still be improved. Electroplating materials onto the silver nanowire, which improves the workable surface area of electrodes and brings them more into compliance with each other, helps improve electrical performance. However, as discussed, this comes at the cost of transparency. The challenge in solving this issue becomes finding a conductor to electroplate that displays good optical transparency and matches the mechanical properties of silver nanowire. PEDOT:PSS is a material that meets all of these requirements and expresses good biocompatibility, meaning it is suitable for direct tissue contact [33,42]. By electroplating PEDOT:PSS onto the gold plated nanowire network, more gaps in the nanowire network that may result in a loss of signal are filled in, but by a transparent material, meaning transmittance should not suffer greatly. PEDOT:PSS coating is a common method of improving the electrical performance and biocompatibility of microelectrodes.

Chapter 5: Conclusion

The objective of this study was to fabricate and characterize the performance of a high density, silver nanowire based, flexible, transparent MEA for simultaneous optoelectronic measurement applications. With a 1 kHz impedance of 29.5 kΩ and an average transmittance of 88.5%, this MEA displays both highly desirable electrical and optical properties, as well as extreme resistance to mechanical strain and oxidation. As current research begins to better acknowledge the multiparametric nature of disease and the idea that one recording method on its own may not provide a full picture, measurement tools which allow for multiple metrics of measurement are becoming increasingly valuable. This work represents an opportunity to close the technological gap between the electrical gold standard of cardiac monitoring and a wide variety of optical imaging techniques to simultaneously visualize electrical, calcium based, and metabolic mechanisms of the heart. There is vast potential for the future growth of this device, including integration of other transparent, flexible materials and greatly increasing the number of measuring channels with ease using laser cutter definition techniques.

References

[1] D. S. Kazi, M. S. V. Elkind, A. Deutsch, *et al*. Forecasting the Economic Burden of Cardiovascular Disease and Stroke in the United States Through 2050: A Presidential Advisory From the American Heart Association. *Circulation*. **150,** 89-101 (2024).

[2] J. Pinnell, S. Turner, S. Howell. Cardiac muscle physiology, *Continuing Education in Anaesthesia Critical Care & Pain*. **7**, 85–88 (2007).

[3] X. Wei, S. Yohannan, J.R. Richards. Physiology, Cardiac Repolarization Dispersion and Reserve. *StatPearls* (2023).

[4] K. Shah, S. Seeley, C. Schulz, et al. Calcium Channels in the Heart: Disease States and Drugs. *Cells.* **11**(6), 943 (2022).

[5] A. M. Wengrowski, S. Kuzmiak-Glancy, R. Jaimes, M. W. Kay. NADH changes during hypoxia, ischemia, and increased work differ between isolated heart preparations. *American Journal of Physiology-Heart and Circulatory Physiology*. **306**:4, H529-H537 (2014).

[6] S. Tibor, R. Marina, R. Richard, *et al.* Golden Standard or Obsolete Method? Review of ECG Applications in Clinical and Experimental Context. *Frontiers in Physiology.* **13** (2022).

[7] Z. Chen, Z. Lin, S. N. Obaid, *et al.* Soft, bioresorbable, transparent microelectrode arrays for multimodal spatiotemporal mapping and modulation of cardiac physiology. *Sci. Adv*. **9**, eadi0757 (2023).

[8] S. Schmidt, W. Li, M. Schubert, *et al.* Novel high-dense microelectrode array based multimodal bioelectronic monitoring system for cardiac arrhythmia re-entry analysis. *Biosensors and Bioelectronics*. **252**, 116120 (2024).

[9] G. Hong, M. C. Lieber. Novel electrode technologies for neural recordings. *Nat. Rev. Neurosci.* **20**, 330– 345 (2019).

[10] F. Wu, E. Stark, P.-C Ku, *et al.* Monolithically Integrated μLEDs on Silicon Neural Probes for High-Resolution Optogenetic Studies in Behaving Animals. *Neuron*. **8**8, 1136-1148 (2015).

[11] S. N. Obaid, Z. Chen, L. Lu. Advanced Electrical and Optical Microsystems for Biointerfacing. *Adv. Intell. Syst. 2* (2020).

[12] Y. Lu, X. Liu, R. Hattori, *et al.* Ultralow Impedance Graphene Microelectrodes with High Optical Transparency for Simultaneous Deep Two-Photon Imaging in Transgenic Mice. *Adv. Funct. Mater.* **28**, 1800002 (2018).

[13] Dong-Wook Park, Jared P. Ness, Sarah K. Brodnick, *et al.* Electrical Neural Stimulation and Simultaneous in Vivo Monitoring with Transparent Graphene Electrode Arrays Implanted in GCaMP6f Mice. *ACS Nano.* **12**, 148-157 (2018).

[14] D. Qi, Z. Liu, Y. Liu, *et al.* Highly Stretchable, Compliant, Polymeric Microelectrode Arrays for In Vivo Electrophysiological Interfacing. *Adv. Mater.* **29**, 1702800 (2017).

[15] J. Park, S. Choi, A. H. Janardhan, *et al.* Electromechanical cardioplasty using a wrapped elasto-conductive epicardial mesh. *Sci. Transl. Med*. **8**, 344ra86 (2016).

[16] J. Zhang, X. Liu, W. Xu, *et al.* Stretchable Transparent Electrode Arrays for Simultaneous Electrical and Optical Interrogation of Neural Circuits in Vivo. *Nano Lett.* **18**, 2903– 2911 (2018).

[17] X. Fan, W. Nie, H. Tsai, *et al.* PEDOT:PSS for Flexible and Stretchable Electronics: Modifications, Strategies, and Applications. *Adv. Sci.* **6,** 1900813 (2019).

[18] G. Ray, C. Jiang, S. Peleshanko, *et al.* Flexible and robust 2D arrays of silver nanowires encapsulated within freestanding layer-by-layer films. *Advanced Functional Materials.* **16**, 2024-2034 (2006).

[19] A. Kumar, M. Kumar, M.S. Goyat, D.K. Avasthi. A review of the latest developments in the production and applications of Ag-nanowires as transparent electrodes. *Materials Today Communications*. **33**, 104433 (2022).

[20] N. T. Quirion *et al*. A soft multimodal optoelectronic array interface for multiparametric mapping of heart function in vivo. *Sci. Adv*. **11**, eads8608 (2025).

[21] M. Parente, M. Helvert, R. F. Hamans, *et al.* Simple and Fast High-Yield Synthesis of Silver Nanowires. *Nano Letters.* **20** (8), 5759-5764 (2020).

[22] S. Coskun, E. Selen Ates, H. Emrah Unalan. Optimization of silver nanowire networks for polymer light emitting diode electrodes. *Nanotechnology*. **24**, 125202 (2013).

[23] Y. Li, & W. X. Wang, Uptake, intracellular dissolution, and cytotoxicity of silver nanowires in cell models. *Chemosphere*, **281**, 130762 (2021).

[24] Y. Wang, X. Yang, & D. Du. Silver Nanowires from Sonication-Induced Scission. *Micromachines*, **10**(1), 29 (2019).

[25] T. Nakagawa, A. Hibara, W. L Hinze, *et al.* Nanoparticle induced formation of self-assembled zwitterionic surfactant microdomains. *RSC Adv*. **10**, 34161-34166 (2020).

[26] G. Hong, C. M. Lieber. Novel electrode technologies for neural recordings. *Nat. Rev. Neurosci.* **20**, 330–345 (2019).

[27] C. Detter, S. Wipper, D. Russ, *et al.* Fluorescent cardiac imaging. *Circulation*. **116,**

1007–1014 (2007).

[28] D. Wang, D. Yang. Optoelectronic and Electrothermal Properties of Transparent Conductive Silver Nanowires Films. *Nanomaterials.* **9,** 512-517 (2019).

[29] A. A. Salam, S. Ebrahim, M. Soliman, *et al.* Preparation of silver nanowires with controlled parameters for conductive transparent electrodes. *Sci. Reports.* **14,** 20986 (2024).

[30] Y. Xia, B. P. Yalagala, A. S. Karimullah, *et al.* Beyond Flexibility: Transparent Silver Nanowire Electrodes on Patterned Surfaces for Reconfigurable Devices. *Adv. Eng. Mater.* **26,** 2301165 (2024).

[31] H. Asfour, A. M Wengrowski, R. Jaimes, *et al.* NADH Fluorescence Imaging of Isolated Biventricular Working Rabbit Hearts. *J. Vis Exp.* **24**, 4115 (2012).

[32] L. Lu. Recent Progress on Transparent Microelectrode-Based Soft Bioelectronic Devices for Neuroscience and Cardiac Research. *ACS Applied Bio Materials.* **6** (5), 1701-1719 (2023).

[33] Z. A. King, C. M. Shaw, S. A. Spanninga, *et al*. Structural, chemical and electrochemical characterization of poly(3,4-ethylenedioxythiophene) (PEDOT) prepared with various counter-ions and heat treatments. *Polymer (Guildf)*. **52**, 1302–1308 (2011).

[34] S. Myllymaa, *et al.* Improving electrochemical performance of flexible thin film electrodes with micropillar array structures. *Meas. Sci. Technol*. **23** 125701 (2012).

[35] M. Thunemann, et al. Deep 2-photon imaging and artifact-free optogenetics through transparent graphene microelectrode arrays. *Nat. Commun*. **9**, 2035 (2018).

[36] N. Kunori, I. Takashima, A transparent epidural electrode array for use in

conjunction with

optical imaging. *J. Neurosci. Methods.* **251**, 130–137 (2015).

[37] J. Zhang, X. Liu, W. Xu, *et al.* Stretchable transparent electrode arrays for simultaneous electrical and optical interrogation of neural circuits in vivo. *Nano Lett.* **18**, 2903–2911 (2018).

[38] S. N. Obaid, R. T. Yin, J. Tian, *et al.* Multifunctional flexible biointerfaces for simultaneous colocalized optophysiology and electrophysiology. *Adv. Funct. Mater.* **30**, 1910027 (2020).

[39] Y. U. Cho, J. Y. Lee, U.-J. Jeong, *et al.* Ultra-low cost, facile fabrication of transparent neural electrode array for electrocorticography with photoelectric artifact-free optogenetics. *Adv. Funct. Mater.* **32,** 2105568 (2022).

[40] M. Thunemann, Y. Lu, X. Liu, *et al.* Deep 2-photon imaging and artifact-free optogenetics through transparent graphene microelectrode arrays. *Nat. Commun.* **9**, 2035 (2018).

[41] W. Wu. Stretchable electronics: functional materials, fabrication strategies and applications. *Science and Technology of Advanced Material.* **20**(1), 187–224 (2019).

[42] A. Susloparova, S. Halliez, S. Begard, *et al.* Low impedance and highly transparent microelectrode arrays (MEA) for in vitro neuron electrical activity probing. S*ensors and Actuators B: Chemical*. **327**, 128895 (2021).